# Realistic One-Boson-Exchange Potentials and Their Applicability in the Shell Model of $O^{18}$

P. S. Ganas*
*University of Florida, Gainesville, Florida 32601*
(Received 13 February 1970)

Realistic, generalized, and regularized, velocity-dependent one-boson-exchange potential models of the nucleon-nucleon interaction are applied to calculate the low-lying energy levels of the nucleus $O^{18}$ in the harmonic-oscillator shell model. In these calculations, we neglect (a) the short-range correlations which, if they were included, would suppress the repulsive core, and (b) core-polarization effects, which take account of the excitations of the $O^{16}$ core. It is found that the shell-model matrix elements are too repulsive, and the energy levels lie too high. Good agreement with experiment is obtained after weakening the $\omega$-meson interaction to compensate for the neglect of the effects (a) and (b). This also provides a simple way of incorporating the effect of the nuclear medium upon the nuclear interaction.

## 1. INTRODUCTION

In recent years the one-boson-exchange-potential model (OBEP) has emerged as a reasonably simple and accurate description of the nucleon-nucleon ($N$-$N$) interaction. This model is based essentially on meson field theory, and many pseudoscalar, vector, and scalar meson models have been found which explain the major features of the $N$-$N$ scattering data.[1] This kind of approach enables the previous almost entirely phenomenological analyses of the $N$-$N$ interaction to be replaced by analyses based more directly on known interactions. All OBEP approaches to date involve some phenomenological modifications, but whereas the purely phenomenological potentials employ 30–50 adjustable parameters in fitting the $N$-$N$ scattering data, generalized forms of one-boson-exchange potentials (GOBEP) achieve comparable fits to the data with fewer than 12 adjustable parameters.

Only a few attempts have been made thus far to apply OBEP to the nuclear many-body problem. Kiang, Preston, and Yip[2] have calculated the state-by-state contributions to the $t$ matrix, using velocity-dependent OBEP derived by Wong,[3] which they have adjusted to be in reasonable agreement with $N$-$N$ scattering data. They find that these are very similar to those found by Bhargava and Sprung for phenomenological potentials. Their work thus indicates that reasonable results will be obtained in nuclear-matter calculations. Ingber[4] and Brueckner and Ingber[5] report excellent results for nuclear matter using a velocity-dependent OBEP associated with $\pi, \omega, \sigma, \eta$, and $\rho$ mesons, and an adaptation of Brueckner, Bethe, and Goldstone techniques in their nuclear-matter calculations. Kohler and McCarthy,[6] using the highly velocity-dependent one-parameter OBEP of Green and Sawada[1] with corrections for the $^1P_1$ phase shift, obtain a binding energy of 7.2 MeV per nucleon for $O^{16}$, in close correspondence with the experimental value of 8 MeV. They used the same reaction matrix, Hartree-Fock calculational methods which for various hard-core phenomenological interactions yielded only 2–3 MeV per nucleon binding. These few studies indicate that a major attack on the nuclear many-body problem should be feasible with OBEP $N$-$N$ interactions.

In this paper we examine for the first time the applicability of OBEP in the shell model of a nucleus. We have chosen $O^{18}$ as a specific example. We consider the GOBEP models I and III of Ueda and Green,[7] referred to as UGI and UGIII, the two-parameter model of Green and Sawada,[8] referred to as GSII, and the most recent model of Bryan and Scott,[9] referred to as BSIII. All these models have $p^2$ velocity-dependent forces and no hard cores. In Sec. 2 we exhibit the various GOBEP models explicitly. In Sec. 3 we briefly describe the technique for calculating the harmonic-oscillator shell-model matrix elements from velocity-dependent GOBEP. In Sec. 4 we present the results of our calculations and compare them with the results from phenomenological potentials.

## 2. ONE-BOSON-EXCHANGE POTENTIAL MODELS

The UGI, UGIII, GSII, and BSIII models employ generalized and regularized Yukawa functions of the form[1]

$$J(r) = (\vec{\tau}_1 \cdot \vec{\tau}_2) G^2 \left( \frac{e^{-\mu r}}{r} - \frac{U^2 - \mu^2}{U^2 - \Lambda^2} \frac{e^{-\Lambda r}}{r} + \frac{\Lambda^2 - \mu^2}{U^2 - \Lambda^2} \frac{e^{-U r}}{r} \right). \tag{2.1}$$

Here $\mu$ is the meson mass, and $\Lambda$ and $U$ are the regularization masses. The quantity $G^2$ is related to the meson-nucleon coupling constant $g^2$ by

$$G^2=\left(\frac{\Lambda^2}{\Lambda^2-\mu^2}\right)^2 g^2 \quad \text{for UGI and UGIII}$$
$$=\left(\frac{\Lambda^2}{\Lambda^2-\mu^2}\right) g^2 \quad \text{for BSIII} \tag{2.2}$$
$$=g^2 \quad \text{for GSII.}$$

The factor $\vec{\tau}_1\cdot\vec{\tau}_2$ is suppressed in the case of $I=0$ mesons. For $I=1$ mesons it has the values

$$\vec{\tau}_1\cdot\vec{\tau}_2=1 \quad \text{for } T=1 \text{ nucleon-nucleon states} \tag{2.3}$$
$$=-3 \quad \text{for } T=0 \text{ nucleon-nucleon states.}$$

Since $O^{18}$ is a $T=1$ nucleus, the relationship (2.3) implies that in calculating the $O^{18}$ levels we may take $\vec{\tau}_1\cdot\vec{\tau}_2=1$ for all mesons.

The regularization mass $U$ is given by the conditions

$$U=\Lambda \quad \text{for UGI and UGIII}$$
$$=\infty \quad \text{for BSIII} \tag{2.4}$$
$$=20M \quad \text{for GSII,}$$

where $M$ is the nucleon mass.

We define various derivatives of the function $J(r)$ given by Eq. (2.1).

$$J_1=\frac{1}{r}\frac{dJ}{dr}, \quad J_2=\frac{1}{r}\frac{dJ_1}{dr}, \tag{2.5}$$

$$\langle\nabla^2 J\rangle=(\vec{\tau}_1\cdot\vec{\tau}_2)G^2\left(\frac{\mu^2 e^{-\mu r}}{r}-\frac{U^2-\mu^2}{U^2-\Lambda^2}\frac{\Lambda^2 e^{-\Lambda r}}{r}\right.$$
$$\left.+\frac{\Lambda^2-\mu^2}{U^2-\Lambda^2}\frac{U^2 e^{-Ur}}{r}\right). \tag{2.6}$$

These derivatives are interrelated

$$\langle\nabla^2 J\rangle=3J_1+r^2 J_2. \tag{2.7}$$

The regularization in Eq. (2.1) is such that the singularities at the origin of the functions $J$, $J_1$, $r^2J_2$, and $\langle\nabla^2 J\rangle$ are all removed.

The four GOBEP models under consideration are based upon the exchange of pseudoscalar ($P$), vector ($V$), and scalar ($S$) mesons. The particular mesons used in each model, and the associated parameters, are listed in Table I. The contributions to the $N$-$N$ potential due to the $P$, $V$, and $S$ interactions are given by the following prescriptions from meson field theory[7]: (In what follows the symbol $p^2$ refers to the operator $-\nabla^2$.)

(i) $P$ contribution

$$V^{(P)}=\left(\tfrac{1}{12}a^2\langle\nabla^2 J\rangle\right)\vec{\sigma}_1\cdot\vec{\sigma}_2+\left(\tfrac{1}{12}a^2 r^2 J_2\right)S_{12}, \tag{2.8}$$

TABLE I. GOBEP models.

| Meson | Tensor | $g^2$ | $f/g$ | $\mu$ (MeV) | $\Lambda$ (MeV) |
|---|---|---|---|---|---|
| | | | (a) UGI | | |
| $\pi$ | $P$ | 14.01 | | 138.7 | 2532.4 |
| $\eta$ | $P$ | 2.73 | | 548.7 | 1184.3 |
| $\rho$ | $V$ | 0.78 | 4.76 | 763 | 1184.3 |
| $\omega$ | $V$ | 8.02 | 0 | 782 | 1184.3 |
| $\pi_v$ | $S$ | 4.11 | | 1016 | 1184.3 |
| $\eta_v$ | $S$ | 4.44 | | 1070 | 1184.3 |
| $\sigma_c$ | $S$ | 1.96 | | 416.1 | 1184.3 |
| | | | (b) UGIII | | |
| $\pi$ | $P$ | 14.61 | | 138.7 | 1299 |
| $\rho$ | $V$ | 0.65 | 5.06 | 763 | 1299 |
| $\omega$ | $V$ | 9.68 | 0 | 782.8 | 1299 |
| $\sigma_1$ | $S$ | 1.01 | | 763 | 1299 |
| $\sigma_0$ | $S$ | 7.32 | | 782.8 | 1299 |
| $\sigma_c$ | $S$ | 1.52 | | 416.1 | 1299 |
| | | | (c) GSII | | |
| $\pi$ | $P$ | 14.7 | | 138.7 | 782.8 |
| $\rho$ | $V$ | 0.65 | 3.75 | 763 | 1500 |
| $\omega$ | $V$ | 23 | 0 | 782.8 | 1500 |
| $\sigma$ | $S$ | 14.7 | | 782.8 | 1500 |
| $\sigma_1$ | $S$ | 0.65 | | 763 | 1500 |
| $\sigma_c$ | $S$ | 2.35 | | 416.1 | 1500 |
| | | | (d) BSIII | | |
| $\pi$ | $P$ | 12.55 | | 138.7 | 1500 |
| $\eta$ | $P$ | 2.6 | | 548.7 | 1500 |
| $\rho$ | $V$ | 1.81 | 1.13 | 763 | 1500 |
| $\omega$ | $V$ | 17.26 | 0 | 782.8 | 1500 |
| $\sigma_1$ | $S$ | 1.65 | | 600 | 1500 |
| $\sigma_0$ | $S$ | 8.19 | | 550 | 1500 |

(ii) $V$ contribution

$$V^{(V)} = \left[J+\tfrac{1}{2}a^2\left(1+\frac{f}{g}\right)\langle\nabla^2 J\rangle\right] + \left[\tfrac{1}{6}a^2\left(1+\frac{f}{g}\right)^2\langle\nabla^2 J\rangle\right]\vec{\sigma}_1\cdot\vec{\sigma}_2 + \tfrac{1}{2}a^2(p^2J+Jp^2)$$
$$+\left[\frac{1}{2}\left(3+4\frac{f}{g}\right)a^2 J_1\right]\vec{1}\cdot\vec{S} - \left[\frac{1}{12}\left(1+\frac{f}{g}\right)^2 a^2 r^2 J_2\right]S_{12}, \tag{2.9}$$

(iii) $S$ contribution

$$V^{(S)} = -J+\tfrac{1}{4}a^2\langle\nabla^2 J\rangle + \tfrac{1}{2}a^2(p^2J+Jp^2) + (\tfrac{1}{2}a^2 J_1)\vec{1}\cdot\vec{S}. \tag{2.10}$$

In the above, $S_{12}$ is the usual tensor operator, and $a=M^{-1}$. To obtain the total $N$-$N$ potential we sum the various one-meson-exchange contributions given by (2.8)–(2.10)

$$V=\sum_p V^{(p)} + \sum_v V^{(v)} + \sum_s V^{(s)}. \tag{2.11}$$

Eq. (2.11) may be placed in the form

$$V = V_C(r) + V_{\sigma\sigma}(r)\vec{\sigma}_1\cdot\vec{\sigma}_2 + V_{\mathrm{VDP}}(r,p^2) + V_{LS}(r)\vec{1}\cdot\vec{S} + V_T(r)S_{12}. \tag{2.12}$$

It is instructive to write out the potential in full for one of the models under consideration, say UGI. We have

$$V_C(r) = J_\rho + \tfrac{1}{2}a^2\left(1+\frac{f_\rho}{g_\rho}\right)\langle\nabla^2 J_\rho\rangle + J_\omega + \tfrac{1}{2}a^2\left(1+\frac{f_\omega}{g_\omega}\right)\langle\nabla^2 J_\omega\rangle - J_{\pi v} + \tfrac{1}{4}a^2\langle\nabla^2 J_{\pi v}\rangle - J_{\eta v} + \tfrac{1}{4}a^2\langle\nabla^2 J_{\eta v}\rangle$$
$$- J_{\sigma c} + \tfrac{1}{4}a^2\langle\nabla^2 J_{\sigma c}\rangle. \tag{2.13}$$

$$V_{\sigma\sigma}(r) = \tfrac{1}{12}a^2\langle\nabla^2 J_\pi\rangle + \tfrac{1}{12}a^2\langle\nabla^2 J_\eta\rangle + \tfrac{1}{6}a^2\left(1+\frac{f_\rho}{g_\rho}\right)^2\langle\nabla^2 J_\rho\rangle + \tfrac{1}{6}a^2\left(1+\frac{f_\omega}{g_\omega}\right)^2\langle\nabla^2 J_\omega\rangle. \tag{2.14}$$

$$V_{\mathrm{VDP}}(r,p^2) = \tfrac{1}{2}a^2(p^2J_\rho + J_\rho p^2) + \tfrac{1}{2}a^2(p^2J_\omega + J_\omega p^2) + \tfrac{1}{2}a^2(p^2J_{\pi v} + J_{\pi v}p^2)$$
$$+\tfrac{1}{2}a^2(p^2J_{\eta v} + J_{\eta v}p^2) + \tfrac{1}{2}a^2(p^2J_{\sigma c} + J_{\sigma c}p^2). \tag{2.15}$$

$$V_{LS}(r) = \tfrac{1}{2}a^2 J_{1,\pi v} + \tfrac{1}{2}a^2 J_{1,\eta v} + \tfrac{1}{2}a^2 J_{1,\sigma c} + \frac{1}{2}\left(3+\frac{4f_\rho}{g_\rho}\right)a^2 J_{1,\rho} + \frac{1}{2}\left(3+\frac{4f_\omega}{g_\omega}\right)a^2 J_{1,\omega}. \tag{2.16}$$

$$V_T(r) = \tfrac{1}{12}a^2 r^2 J_{2,\pi} + \tfrac{1}{12}a^2 r^2 J_{2,\eta} - \frac{1}{12}\left(1+\frac{f_\rho}{g_\rho}\right)^2 a^2 r^2 J_{2,\rho} - \frac{1}{12}\left(1+\frac{f_\omega}{g_\omega}\right)^2 a^2 r^2 J_{2,\omega}. \tag{2.17}$$

The radial components for the other three models are given by similar expressions to Eqs. (2.13)–(2.17).

## 3. CALCULATION OF MATRIX ELEMENTS FROM OBEP

In the calculation of low-lying states, the nucleus $O^{18}$ may be considered basically as an inert $O^{16}$ core plus two valence neutrons confined in the $s$-$d$ shell. Then to obtain the spectrum we simply diagonalize the two-nucleon secular matrix in the $s$-$d$ shell. As is conventional to assume, the $O^{16}$ core provides harmonic-oscillator potential well for the two valence neutrons. As a first approximation we take the residual interaction to be the one-boson-exchange potential.

On account of the regularization in Eq. (2.1), the total potential, Eq. (2.12), is nonsingular at the origin. For a nonsingular potential $V$, the shell-model matrix element in $jj$ coupling can be written as

$$(abJT|V|cdJT)=\left[\frac{(2j_a+1)(2j_b+1)(2j_c+1)(2j_d+1)}{(1+\delta_{ab})(1+\delta_{cd})}\right]^{1/2}$$

$$\times\sum_{LL'S}[(2L+1)(2L'+1)]^{1/2}(2S+1)\begin{Bmatrix} l_a & \frac{1}{2} & j_a \\ l_b & \frac{1}{2} & j_b \\ L & S & J \end{Bmatrix}\begin{Bmatrix} l_c & \frac{1}{2} & j_c \\ l_d & \frac{1}{2} & j_d \\ L' & S & J \end{Bmatrix}(-1)^{L+L'}$$

$$\times\sum_{\substack{nln'l'\\ N\mathcal{L}}}\langle nlN\mathcal{L}L|n_a l_a n_b l_b L\rangle\langle n'l'N\mathcal{L}L'|n_c l_c n_d l_d L'\rangle(-1)^{l+l'}[1-(-1)^{l+S+T}]$$

$$\times\sum_{\mathcal{J}}U(\mathcal{L}lJS;L\mathcal{J})U(\mathcal{L}l'JS;L'\mathcal{J})(nlST\mathcal{J}|V|n'l'ST\mathcal{J}). \tag{3.1}$$

The index $a$ stands for the quantum numbers $n_a$, $l_a$, $j_a$ of a spherical oscillator orbital.[10] The ket $|abJT)$ represents a normalized and antisymmetrized state where $a$ and $b$ couple to total angular momentum $J$ and isotopic spin $T$. The arrays in large curly brackets are $9j$ symbols.[11] The bracket $\langle nlN\mathcal{L}L|n_a l_a n_b l_b L\rangle$ is the Brody-Moshinsky transformation bracket between the lab frame and the c.m. and relative frame; $nl$ and $N\mathcal{L}$ are, respectively, the relative and c.m. oscillator quantum numbers.[12] We note that $l(l')$ and $S$ couple to $\mathcal{J}$. The $U$ coefficient is the normalized Racah coefficient

$$U(\mathcal{L}lJS;L\mathcal{J})=[(2L+1)(2\mathcal{J}+1)]^{1/2}W(\mathcal{L}lJS;L\mathcal{J}). \tag{3.2}$$

The integral $(nlST\mathcal{J}|V|n'l'ST\mathcal{J})$ may be conveniently separated into an angular-spin part and a radial part, namely,

$$(nlST\mathcal{J}|V|n'l'ST\mathcal{J})=\sum_i(lS\mathcal{J}|A_i|l'S\mathcal{J})(nl|V_i(r)|n'l'), \tag{3.3}$$

where all the radial dependence of the $i$th component of $V$ is contained in $V_i(r)$. The index $T$ has been absorbed in $V_i(r)$ as usual.

The GOBEP models under consideration have central, spin-spin, spin-orbit, tensor, and $p^2$ velocity-dependent components. Ueda and Green have also introduced a phenomenological $\vec{l}^2$ component into some of their models.[7,13] It has the form $V_{LL}(r)\vec{l}^2$ where

$$V_{LL}(r)=\tfrac{1}{2}(1+P)J(r). \tag{3.4}$$

Here $P$ is the parity operator for the two-nucleon state, and $J(r)$ is a regularized Yukawa potential. This interaction is constructed to act only in even states for the practical reason of improving the fits to the $^1D_2$ and $^3D_2$ phase shifts at high energy.

The angular-spin parts can be readily obtained for the GOBEP models.

$$(lS\mathcal{J}|\vec{\sigma}_1\cdot\vec{\sigma}_2|l'S\mathcal{J})=(\delta_{S1}-3\delta_{S0})\delta_{ll'}. \tag{3.5}$$

$$(lS\mathcal{J}|\vec{l}\cdot\vec{S}|l'S\mathcal{J})=\delta_{ll'}\delta_{S1}\tfrac{1}{2}[\mathcal{J}(\mathcal{J}+1)-l(l+1)-2]. \tag{3.6}$$

$$(lS\mathcal{J}|S_{12}|l'S\mathcal{J})=\delta_{S1}(-1)^{1-\mathcal{J}}[24(2l+1)(2l'+1)]^{1/2}\times W(lSl'S;\mathcal{J}2)\langle l200|l'0\rangle. \tag{3.7}$$

$$(lS\mathcal{J}|\vec{l}^2|l'S\mathcal{J})=\delta_{ll'}l(l+1). \tag{3.8}$$

Here $\langle l200|l'0\rangle$ is a Clebsch-Gordan coefficient.[11] The relative-motion matrix elements $(nl|V(r)|n'l')$ are very conveniently evaluated by obtaining their Talmi integral expansion

$$(nl|V(r)|n'l')=\sum_p B(nl,n'l',p)I_p[V]. \tag{3.9}$$

General alegbraic formulas for the $B$ coefficients are given by Brody and Moshinsky.[12] The functional $I_p[V]$ is called the Talmi integral and is defined by

$$I_p[V]=\frac{2}{(p+\frac{1}{2})!}\int_0^\infty e^{-x^2}x^{2p+2}V(\sqrt{2}\lambda x)dx, \tag{3.10}$$

where $\lambda$ is the size parameter of the harmonic oscillator. The value $\lambda=1.71$ F is commonly used in calculations of the $O^{18}$ levels.[14,15]

The relative-motion matrix elements for $p^2$

velocity-dependent forces can also be evaluated from a Talmi integral expansion

$$\left(nl\left|\frac{p^2}{2M}V(r)+V(r)\frac{p^2}{2M}\right|n'l\right)$$
$$=\frac{\hbar^2}{2M\lambda^2}\sum_p G(nl,n'l,p)I_p[V]. \quad (3.11)$$

The $G$ coefficients are expressible in terms of the $B$ coefficients.[15]

We see finally that the shell-model matrix elements from a regularized one-boson-exchange potential are calculated by obtaining the Talmi integral expansions of the potential components. Thus, we can compare the effects of different potentials in the shell model by making a direct comparison between their Talmi integrals. In particular, if the corresponding Talmi integrals from two potentials are equal, then the two potentials give rise to the same matrix elements and the same energy levels.

TABLE II. Talmi integrals from OBEP for $O^{18}$. Units are MeV.

(a) Singlet even Talmi integrals $I_p[V_C-3V_{\sigma\sigma}]$

| $p$ | UGI | UGIII | BSIII | GSII | AMG |
|---|---|---|---|---|---|
| 0 | −0.4506 | −1.6375 | +3.8003 | +1.2641 | −6.8883 |
| 1 | −1.8765 | −1.7475 | −1.4241 | −1.4190 | −1.7283 |
| 2 | −0.5714 | −0.5423 | −0.4597 | −0.5204 | −0.5368 |
| 3 | −0.2298 | −0.2258 | −0.1871 | −0.2263 | −0.2175 |
| 4 | −0.1161 | −0.1177 | −0.0968 | −0.1180 | −0.1094 |

(b) Triplet odd Talmi integrals $I_p[V_C+V_{\sigma\sigma}]$

| $p$ | UGI | UGIII | AMG |
|---|---|---|---|
| 0 | −6.0719 | −7.1361 | +0.6624 |
| 1 | −0.0080 | −0.0156 | +0.2243 |
| 2 | −0.0120 | +0.0132 | +0.1033 |
| 3 | +0.0125 | +0.0249 | +0.0563 |
| 4 | +0.0181 | +0.0234 | +0.0330 |

(c) Spin-orbit Talmi integrals $I_p[V_{LS}]$

| $p$ | UGI | UGIII | AMG |
|---|---|---|---|
| 0 | −13.9040 | −16.7940 | −5.1374 |
| 1 | −0.6632 | −0.7342 | −0.8052 |
| 2 | −0.0492 | −0.0504 | −0.1262 |
| 3 | −0.0052 | −0.0050 | −0.0198 |
| 4 | −0.0008 | −0.0007 | −0.0031 |

(d) Tensor Talmi integrals $I_p[V_T]$

| $p$ | UGI | UGIII | AMG |
|---|---|---|---|
| 0 | 4.4872 | 0.7172 | 2.6051 |
| 1 | 0.8479 | 0.7763 | 0.8821 |
| 2 | 0.3236 | 0.3374 | 0.4063 |
| 3 | 0.1503 | 0.1589 | 0.2215 |
| 4 | 0.0792 | 0.0839 | 0.1300 |

(e) Velocity-dependent-potential Talmi integrals $I_p[V_{VDP}]$

| $p$ | UGI | UGIII | AMG |
|---|---|---|---|
| 0 | 0.1341 | 0.1596 | 0.1701 |
| 1 | 0.0116 | 0.0125 | 0.0130 |

## 4. RESULTS AND DISCUSSION

The aim of the present calculations is to determine whether the velocity-dependent one-boson-exchange potentials (UGI, UGIII, GSII, BSIII) are applicable in the shell model of a nucleus, $O^{18}$ being chosen as a specific example for discussion. We are interested in comparing our results with those from a velocity-dependent phenomenological potential, e.g., that of A. M. Green. This potential has been extensively applied to the shell model[16-18] and is referred to hereafter as the AMG potential.

For $O^{18}$ only the singlet even (SE) and triplet odd (TO) potential components contribute. We have computed the Talmi integrals from the definition (3.10) and the radial dependences (2.13)–(2.17). Our results are displayed in Table II. With the exception of $p=0$, the Talmi integrals from the GOBEP models substantially agree with one another, respectively, and with the values obtained from the AMG potential. Since the TO matrix elements are independent of the $p=0$ Talmi integrals (by virtue of the condition[12] $p \geq l$), we expect the TO matrix elements from the GOBEP models to be rather similar to one another, respectively, and to the TO matrix elements from the AMG potential. On the other hand, the SE matrix ele-

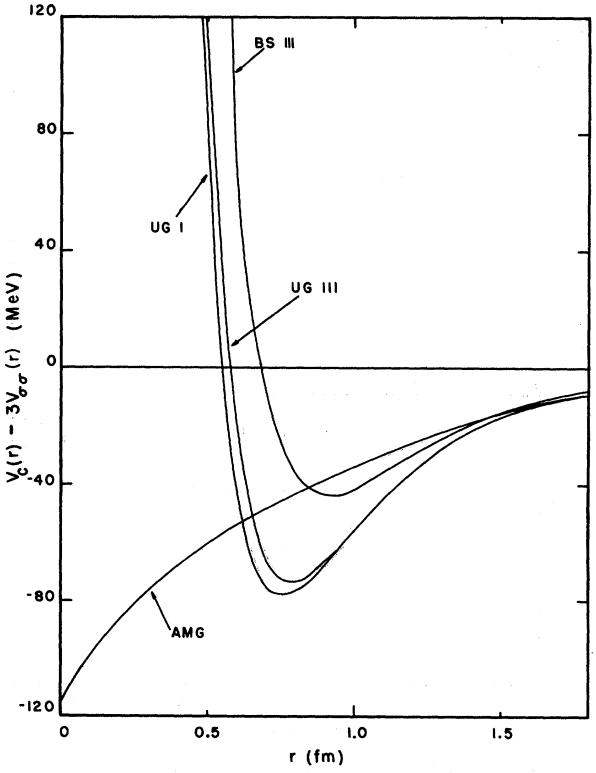


FIG. 1. The singlet even static potential.

ments are very sensitive to the $p=0$ Talmi integral of the SE static potential; and since this Talmi integral is much less attractive for the GOBEP models than for the AMG potential, we expect the SE matrix elements to exhibit much more repulsion with GOBEP than with the phenomenological potential. In Table III we have decomposed the matrix element

$$(1d_{5/2}{}^2J|V|\,1d_{5/2}{}^2J). \tag{4.1}$$

The results in Table III confirm our expectations that the TO contributions are essentially the same for both GOBEP and AMG models, whereas the static SE contributions are much more repulsive with GOBEP than with the AMG potential.

In Fig. 1 we have plotted the SE static component of GOBEP. Except at very short ranges, the GOBEP models behave like the phenomenological model. At short ranges, the GOBEP models become strongly repulsive but remain finite at the origin; in other words they have a soft core. In addition to the soft core there is present a nonstatic repulsion which arises from the $p^2$ velocity-dependent force, and is usually compared to a hard core. In Figs. 2 and 3 we have plotted the Talmi integrands for the SE static potential. With the notable exception of $p=0$, they are relatively insensitive to the behavior of the potential at very short ranges.

In Table IV we display the energy matrices. The matrix elements exhibit much more repulsion with GOBEP than with the phenomenological potential. The energy levels from GOBEP are shown in Fig. 4. They lie much higher than the levels from the AMG potential, and are incorrectly ordered with respect to experiment.

Finally we consider the question of how to modify GOBEP in order to improve the agreement with the experimental levels of $O^{18}$. In Table V we have decomposed the static SE Talmi integrals into individual meson contributions. For the $p=0$ Talmi integral the dominant repulsive contribution comes from the $\omega$ meson, while the dominant attractive contribution comes from the light scalar meson in the case of UGI, and from the heavy scalar meson in the case of UGIII. Thus, in order to strengthen the $p=0$ Talmi integral, we need to reduce the coupling constant of the $\omega$ meson and/or increase the coupling constant of the appropriate scalar meson. It is interesting to note that any change in the $\omega$-meson interaction affects all the potential components, as Eqs. (2.13)–(2.17) show. We have performed searches on the low-lying experimental levels of $O^{18}$ using an automatic

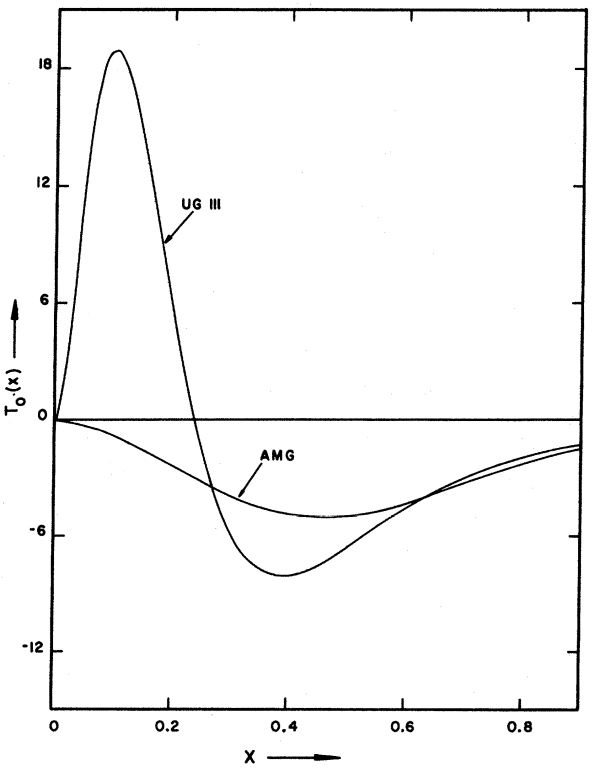


FIG. 2. Talmi integrand $T_0(x)=e^{-x^2}x^2V(\sqrt{2}\lambda x)$, where $V(x)=V_c(x)-3V_{\sigma\sigma}(x)$.

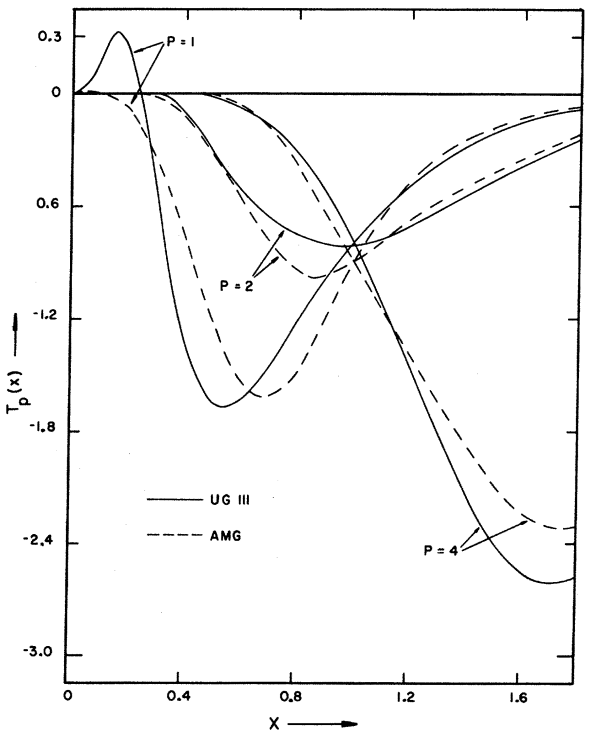


FIG. 3. Talmi integrands $T_p(x)=e^{-x^2}x^{2p+2}V(\sqrt{2}\lambda x)$ for $p>0$, where $V(x)=V_c(x)-3V_{\sigma\sigma}(x)$.

TABLE III. Decomposition of $(1d_{5/2}{}^2J|V|1d_{5/2}{}^2J)$. Units are MeV. The symbols CSE, VSE denote the static singlet even and velocity-dependent singlet even contributions, respectively. The symbols CTO, VTO, TTO, LS denote respectively the static central triplet odd, velocity-dependent central triplet odd, tensor odd and spin-orbit contributions.

| | $J=0$ | | $J=2$ | | $J=4$ | |
|---|---|---|---|---|---|---|
| | UGI | AMG | UGI | AMG | UGI | AMG |
| CSE | +1.797 | −3.461 | +0.099 | −1.080 | −0.071 | −0.552 |
| VSE | 1.191 | 1.568 | 0.243 | 0.316 | 0.058 | 0.074 |
| $l^2$ force | −0.001 | | −0.009 | | −0.001 | |
| Total SE | 2.987 | −1.893 | 0.333 | −0.764 | −0.014 | −0.478 |
| CTO | 0.015 | 0.093 | 0.017 | 0.144 | 0.002 | 0.112 |
| VTO | 0.138 | 0 | 0.159 | 0 | 0.050 | 0 |
| TTO | 0.750 | 0.732 | 0.049 | 0.055 | 0.140 | 0.132 |
| LS | 0.419 | 0.451 | −0.226 | −0.240 | −0.072 | −0.102 |
| Total TO | 1.322 | 1.276 | −0.001 | −0.071 | 0.120 | 0.142 |
| Total | 4.309 | −0.617 | 0.332 | −0.835 | 0.106 | −0.336 |

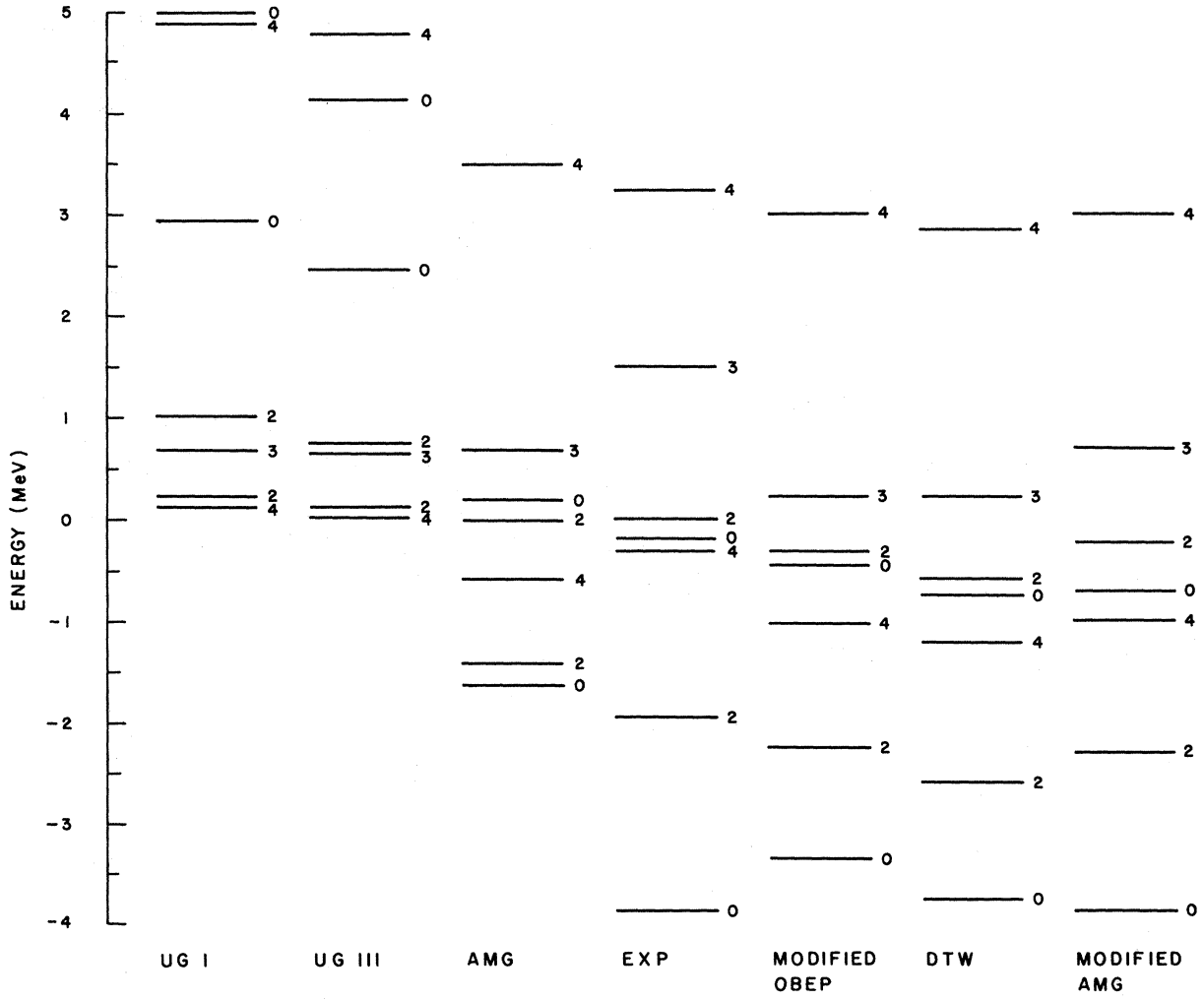


FIG. 4. Level schemes for $O^{18}$.

TABLE IV. Energy matrices for $O^{18}$. The first row of each block corresponds to GOBEP model UGIII, while the second row corresponds to the AMG potential. Units are MeV.

$J=0$

| | $d_{5/2}^2$ | $s_{1/2}^2$ | $d_{3/2}^2$ |
|---|---|---|---|
| $d_{5/2}^2$ | 3.394<br>−0.616 | 0.852<br>−0.545 | 0.256<br>−3.110 |
| $s_{1/2}^2$ | | 3.218<br>−0.080 | 0.696<br>−0.445 |
| $d_{3/2}^2$ | | | 13.450<br>10.813 |

$J=3$

| | $d_{5/2}s_{1/2}$ | $d_{5/2}d_{3/2}$ |
|---|---|---|
| $d_{5/2}s_{1/2}$ | 0.670<br>0.680 | −0.114<br>−0.087 |
| $d_{5/2}d_{3/2}$ | | 4.717<br>4.768 |

$J=4$

| | $d_{5/2}^2$ | $d_{5/2}d_{3/2}$ |
|---|---|---|
| $d_{5/2}^2$ | 0.009<br>−0.336 | −0.229<br>−1.027 |
| $d_{5/2}d_{3/2}$ | | 4.746<br>3.203 |

$J=2$

| | $d_{5/2}^2$ | $d_{5/2}s_{1/2}$ | $d_{5/2}d_{3/2}$ | $s_{1/2}d_{3/2}$ | $d_{3/2}^2$ |
|---|---|---|---|---|---|
| $d_{5/2}^2$ | 0.094<br>−0.834 | 0.138<br>−0.479 | 0.212<br>−0.396 | 0.019<br>−0.553 | 0.126<br>−0.623 |
| $d_{5/2}s_{1/2}$ | | 0.821<br>−0.106 | 0.352<br>−0.087 | −0.695<br>−1.543 | −0.256<br>−0.815 |
| $d_{5/2}d_{3/2}$ | | | 5.390<br>4.915 | −0.298<br>−0.699 | −0.250<br>−0.801 |
| $s_{1/2}d_{3/2}$ | | | | 6.185<br>5.604 | 0.457<br>0.128 |
| $d_{3/2}^2$ | | | | | 10.567<br>10.127 |

TABLE V. Decomposition of Talmi integrals from OBEP for $O^{18}$. Units are MeV.

(a) UGI

| Meson | $p=0$ | $p=1$ | $p=2$ | $p=3$ | $p=4$ |
|---|---|---|---|---|---|
| $\pi$ | +2.7986 | −0.6261 | −0.3066 | −0.1657 | −0.0981 |
| $\eta$ | +0.0959 | −0.0487 | −0.0094 | −0.0018 | −0.0004 |
| $\pi_v$ | −4.5089 | −0.2281 | −0.0158 | −0.0014 | −0.0001 |
| $\eta_v$ | −4.4081 | −0.2139 | −0.0142 | −0.0012 | −0.0001 |
| $\sigma_c$ | −11.0588 | −1.4142 | −0.2633 | −0.0626 | −0.0176 |
| $\rho$ | +2.3051 | −0.3571 | −0.0561 | −0.0079 | −0.0012 |
| $\omega$ | +14.3254 | +1.0116 | +0.0941 | +0.0108 | +0.0015 |
| Total | −0.4506 | −1.8765 | −0.5714 | −0.2298 | −0.1161 |
| AMG | −6.8883 | −1.7283 | −0.5368 | −0.2175 | −0.1094 |

(b) UGIII

| Meson | $p=0$ | $p=1$ | $p=2$ | $p=3$ | $p=4$ |
|---|---|---|---|---|---|
| $\pi$ | +2.8007 | −0.5601 | −0.3195 | −0.1754 | −0.1040 |
| $\sigma_1$ | −1.9297 | −0.1169 | −0.0101 | −0.0011 | −0.0002 |
| $\sigma_0$ | −13.3261 | −0.7848 | −0.0658 | −0.0071 | −0.0009 |
| $\sigma_c$ | −8.6457 | −1.0653 | −0.1959 | −0.0464 | −0.0130 |
| $\rho$ | +2.0254 | −0.3617 | −0.0513 | −0.0068 | −0.0010 |
| $\omega$ | +17.4378 | +1.1413 | +0.1004 | +0.0111 | +0.0015 |
| Total | −1.6375 | −1.7475 | −0.5423 | −0.2258 | −0.1177 |
| AMG | −6.8883 | −1.7283 | −0.5368 | −0.2175 | −0.1094 |

search routine. Starting from UGIII and letting $g_\omega^2$ vary, we obtain an optimum fit to the $O^{18}$ levels for $g_\omega^2 = 5.81$, which corresponds to a 40% reduction. The corresponding energy levels are shown in Fig. 4 under the label "modified OBEP." They are correctly ordered and the spacings are reasonable. They are similar to the levels obtained by Dawson, Talmi, and Walecka (DTW)[19] from the Brueckner-Gammel-Thaler potential, and also the levels obtained by Ganas and McKellar[17] who modified the AMG potential. We find that the same levels are obtained by letting $g_\omega^2$ and $g_{\sigma 0}^2$ vary together. The optimum values in this case are $g_\omega^2 = 8.16$ (a 15% reduction), and $g_{\sigma 0}^2 = 9.88$ (a 35% increase). It is noteworthy that these modifications are of the same order as those made by Ganas and McKellar[17,18] to the phenomenological AMG potential in order to fit the low-energy spectra of light, medium, and heavy nuclei.

The calculations with the GSII and BSIII models were discontinued when it became apparent from Table II that agreement with experiment would be

even more unlikely with these models than with UGI and UGIII.

## 5. CONCLUSION

The aim of the present calculations has been to test the applicability of the one-boson-exchange potential in the shell model of a finite nucleus. The potential models which we have considered are velocity dependent and nonsingular. On computing the $s$-$d$-shell matrix elements for $O^{18}$ using the standard method of calculation for nonsingular potentials, we find that the matrix elements exhibit too much repulsion, mainly on account of the soft core. This suggests that it would be more desirable to work with the Brueckner reaction matrix rather than the potential matrix as we have done. In other words, even though the one-boson-exchange potentials are nonsingular, they have sufficiently strong short-range repulsion that it becomes necessary to use Brueckner theory. When this is done, the short-range correlations suppress the repulsive core. Another major effect which has been neglected is core polarization; the $O^{16}$ core is not inert, and corrections due to its excitation must be taken into account. Extensive Brueckner-type calculations on finite nuclei, including core-polarization effects, have been performed by Kuo and Brown[20] for a phenomenological hard-core potential. It would be interesting to repeat the calculations of Kuo and Brown using a meson-theoretic velocity-dependent potential.

We have attempted to compensate for the omission of short-range correlation effects and core-polarization effects by readjusting the coupling constants of the potential so as to give agreement with the experimental spectrum of $O^{18}$. We find empirically that it is necessary to reduce the $\omega$-meson coupling constant by 40% in order to achieve good agreement with experiment. This is not a surprising result, because the $\omega$ meson is mainly responsible for the repulsive core of the potential. This result is suggestive of the Scott-Moszkowski separation-method technique which has proved so useful in the treatment of hard-core potentials.

The one-boson-exchange potentials are determined by fitting the two-nucleon data with phase shifts found from the Schrödinger equation. Arndt, Bryan, and MacGregor[21] have discussed the one-boson-exchange potential in the Born approximation, and have determined coupling constants which give good fits to the two-nucleon data in the Born approximation, $S$ waves being excluded. Since we have calculated the $s$-$d$-shell matrix elements in the lowest-order Born approximation, we might expect to obtain better agreement with experiment by using the parameters of Arndt, Bryan, and MacGregor.[22] Indeed the $\omega$-meson coupling constant quoted by these authors is quite close to the value which we have obtained by fitting to the $O^{18}$ levels.

We have seen that the various one-boson-exchange models as well as the phenomenological model behave in a similar way except in the region of the repulsive core. However, such differences are expected to manifest themselves only weakly in the shell-model matrix elements if the potentials are treated in the Brueckner $G$-matrix approximation. In these circumstances it seems likely that the various potential models will all lead to essentially the same results when applied to the nuclear shell model.

## ACKNOWLEDGMENTS

I would like to thank Professor Alex Green for offering helpful comments and giving enthusiastic support to this work. I would also like to thank Dr. Alexander Gersten for several illuminating discussions. It is a pleasure to thank Professor Ron Bryan for reading the manuscript very critically and suggesting improvements. The work was supported in part by the Air Force Office of Scientific Research (OAR) Grant No. AFOSR-68-1397.

---

*Address after 31 August: California State College at Los Angeles, Los Angeles, California 90032.

[1]A. E. S. Green and T. Sawada, Rev. Mod. Phys. 39, 594 (1967); Nucl. Phys. B2, 267 (1967).

[2]D. Kiang, M. A. Preston, and P. Yip, Phys. Rev. 107, 907 (1968).

[3]D. Y. Wong, Nucl. Phys. 55, 212 (1964).

[4]L. Ingber, Phys. Rev. 174, 1250 (1968).

[5]K. A. Brueckner and L. Ingber, J. Phys. Soc. Japan Suppl. 24, 616 (1968).

[6]R. J. McCarthy and H. S. Kohler, Phys. Rev. Letters 20, 671 (1968).

[7]T. Ueda and A. E. S. Green, Phys. Rev. 174, 1304 (1968).

[8]A. E. S. Green and T. Sawada, J. Phys. Soc. Japan Suppl. 24, 616 (1968).

[9]R. A. Bryan and B. L. Scott, Phys. Rev. 177, 1435 (1969).

[10]A. de-Shalit and I. Talmi, *Nuclear Shell Theory* (Academic Press Inc., New York, 1963).

[11]D. M. Brink and G. R. Satchler, *Angular Momentum* (Oxford University Press, New York, 1962).

[12]T. A. Brody and M. Moshinsky, *Tables of Transformation Brackets for Nuclear Shell-Model Calculations* (Dirección General de Publicaciones, Universidad Nacional de México, Ciudad Universitaria, Mexico, D. F., 1960).
[13]T. Ueda and A. E. S. Green, Nucl. Phys. B10, 289 (1969).
[14]C. W. Lee and E. Baranger, Nucl. Phys. 79, 385 (1966).
[15]B. H. J. McKellar, Phys. Rev. 134, B1190 (1964).
[16]P. S. Ganas and B. H. J. McKellar, Phys. Rev. 175, 1409 (1968).
[17]P. S. Ganas and B. H. J. McKellar, Nucl. Phys. A120, 545 (1968).
[18]P. S. Ganas and B. H. J. McKellar, Phys. Rev. 180, 953 (1969).
[19]J. F. Dawson, I. Talmi, and J. D. Walecka, Ann. Phys. (N. Y.) 18, 339 (1962).
[20]T. T. S. Kuo and G. E. Brown, Nucl. Phys. 85, 40 (1966).
[21]R. A. Arndt, R. Bryan, and M. H. MacGregor, Phys. Letters 21, 314 (1966).
[22]The author thanks Professor Bryan for this remark.

PHYSICAL REVIEW C VOLUME 2, NUMBER 1 JULY 1970

# Magnetic Hyperfine Structure of Muonic Atoms*

John Johnson† and Raymond A. Sorensen
*Carnegie-Mellon University, Pittsburgh, Pennsylvania 15213*
(Received 22 January 1970)

Magnetic hyperfine structure in muonic x rays is calculated for several models of the nuclear magnetism and compared to experimental values for $^{115}$In, $^{127}$I, $^{133}$Cs, $^{139}$La, $^{141}$Pr, $^{151}$Eu, $^{203}$Tl, $^{205}$Tl, and $^{209}$Bi. The results are excellent for the realistic models in most cases, and all but one of the nine cases agree within better than two standard deviations with the experiments. For the realistic models, the hyperfine energy is substantially reduced (by about 30% in most cases) from its point-nucleus value. In these models, the single-particle magnetism distribution is modified by the addition of configurations resulting from various residual nuclear interactions, the interaction strength being adjusted in each case to produce the experimental value for the magnetic moment.

## I. INTRODUCTION

The hyperfine splitting of levels in electronic and muonic atoms is due to the interaction of the nuclear magnetism with the magnetic field of the orbiting electron or muon. The energy of interaction depends on the relative orientation of the nuclear magnetism and the field. For a point dipole of strength $\vec{\mu}$ in a field $B$ the energy is

$$W = -\vec{\mu} \cdot \vec{B}. \quad (1)$$

Two isotopes have a nearly identical electronic structure, and therefore the magnetic field at the nucleus is the same for each isotope. The hyperfine splitting will be different for the two isotopes because the nuclear moments are different. However, the ratio of the nuclear moments should equal the ratio of the splittings if the nucleus is a point dipole.

In 1947 Bitter[1] made a very accurate measurement of the ratio of the magnetic moments of two rubidium isotopes using magnetic-resonance techniques. This ratio differed slightly from the ratio of the hyperfine structure splittings, indicating Eq. (1) is incorrect. Bitter[2] suggested that the discrepancy was due to an extended distribution of nuclear magnetism. Bohr and Weisskopf[3] made the first detailed calculations of this "hyperfine anomaly" in 1950, and the effect is sometimes called the "Bohr-Weisskopf" effect. Since then, many more hyperfine anomalies have been measured, making possible a systematic investigation of the effect.[4]

More recently, the hyperfine structure of muonic atoms has been measured for several cases.[5-9] A muonic atom is formed by stopping negatively charged muons in a target. The muon is captured by an atom and makes Auger and radiative (x-ray) transitions down through the atomic orbits until it reaches the 1s state. It is then either captured by the nucleus via the weak interaction, or it decays. Since the muon is 206 times heavier than an electron, its orbits are 206 times closer to the nucleus than the equivalent electron orbits. The muon energy levels are thus quite sensitive to the nuclear structure. By observing the x rays given off in the transitions, one can learn something about nuclear structure. In particular, the hyperfine structure of the x rays depends on the distribution of magnetism of the nucleus and differs from that calculated for a point nucleus by as much as 50%.

The hyperfine structure in muonic atoms is usually observed as a broadening of the x ray given